

Real-Time *Operando* Diffraction Imaging of La-Sr/CaO During the Oxidative Coupling of Methane

Dorota Matras^{1,2*}, Simon D.M. Jacques^{3*}, Hamid R. Godini⁴, Mohammadali Khadivi⁴, Jakub Drnec⁵, Agnieszka Poulain⁵, Robert J. Cernik¹ and Andrew M. Beale^{2,3,6*}

¹ School of Materials, University of Manchester, Manchester, Lancashire M13 9PL, UK.

² Research Complex at Harwell, Harwell Science and Innovation Campus, Rutherford Appleton Laboratory, Didcot, Oxon, OX11 0FA, UK.

³ Finden Ltd, Merchant House, 5 East St Helen Street, Abingdon, OX14 5EG, UK.

⁴ Technische Universität Berlin, Straße des 17 Juni 135, Sekr. KWT-9, D-10623 Berlin, Germany.

⁵ ESRF- The European Synchrotron, Grenoble, 38000 France.

⁶ Department of Chemistry, University College London, 20 Gordon Street, London, WC1H 0AJ, UK.

Correspondance email: dorota.matras@rc-harwell.ac.uk, simon@finden.co.uk,
andrew.beale@ucl.ac.uk

Abstract

An La-Sr/CaO catalyst has been chemically imaged during activation and under *operando* conditions during the oxidative coupling of methane reaction (OCM) at high temperature using X-ray diffraction computed tomography (XRD-CT) in combination with full pattern Rietveld refinement. At room temperature the main components of the catalyst were present as carbonates and hydroxides. During the activation stage (temperature ramp) they decomposed,

forming La_2O_3 , SrO and mixed CaO-SrO oxides. Under the OCM reaction conditions, the predominant phases present were (~20 % wt.) La_2O_3 and CaO-SrO (~45 % wt.) and these remained stable throughout the entire reaction, whereas SrO , formed during activation, reacted with produced CO_2 leading to formation of SrCO_3 (~ 35 % wt). Two polymorphs of SrCO_3 , orthorhombic and rhombohedral, were found to be stable under reaction conditions although the extent to which these phases were observed varied spatially and temporally with reactant gas composition. The presence of the high temperature rhombohedral polymorph can be associated with higher combustion activity and since the Rietveld analysis is performed on a pixel-by-pixel basis it is possible to observe, for the first time, domains of differing activity within the reactor.

1. Introduction

Since the first publication of Keller and Bhasin the oxidative coupling of methane (OCM) has been a widely studied process, which can offer an alternative way to produce added value hydrocarbons from natural gas via an exothermic catalytic reaction between methane and oxygen¹. The continued depletion of oil resources coupled with a great increase in methane availability (particularly through shale gas exploitation) has led to a growing interest and economic imperative for looking at alternative processes for the production of chemicals in general and specifically ethylene, an important platform chemical². However, as is typical for the selective oxidation reactions, the OCM process presents conversion-selectivity problems. High methane conversions are obtained when feeding the reactor with a high flow of oxygen, which results in poor selectivity for desired C_{2+} products and a large amount of undesired combustion products: carbon monoxide and carbon dioxide. However, the OCM process is still believed to offer an economically viable solution of ethylene production³. During the past 30 years, most of the research has focused on increasing the C_{2+} yield by developing and formulating new catalysts; a wide variety of catalysts based on the metal oxides, alkali, alkaline

earth, rare earth and transition metal oxides⁴⁻⁷. Among them, the La-Sr/CaO catalyst was found to provide a good yield and C₂₊ productivity as well as great stability after 90 hours of reaction⁴. According to Olivier et al. the best performing La-Sr/CaO catalyst provides 34 % of methane conversion and C₂₊ yield of 19 %⁴.

Simple oxides present in the catalyst material (La₂O₃, SrO and CaO) are found to easily absorb H₂O and CO₂ when exposed to air, which leads to formation of various hydroxides, carbonates and oxocarbonates⁸⁻¹⁰. When reaching high temperatures i.e. 800 °C, in which the OCM process is usually performed¹¹, the catalyst material is believed to undergo chemical and structural changes. However, the final composition of the catalyst consists of simple oxides¹². In the study performed by Taylor and Schrader it was suggested that the catalytic activity of La₂O₃ catalyst depends on its composition as well as on the different lanthanum compounds that were formed during the temperature ramp and OCM reaction¹².

The improvement of reactor design and studies of different reactors concepts have also been conducted, aiming to improve the C₂₊ yield. Among them, the concept of the catalytic membrane reactor (CMR), with the oxygen permeable membrane, is believed to offer an improved yield in OCM process¹³. As reported by Bhatia et al. the application of a CMR for the OCM process could provide as much as a 35 % C₂₊ yield with methane conversions of 52 %¹⁴. However, it is believed that research still needs to focus on further development and formulation of better performing catalytic materials. For that matter an understanding of how the catalyst evolves under operating conditions and its stability over time periods necessary to realise commercial application (i.e. several days – months).

In catalysis, the ultimate aim is to understand the structural and chemical variation within a catalyst, occurring at different length scales and through the entire catalyst lifetime¹⁵. Deeper understanding of the relationship between the catalyst structure and its activity can be obtained

through the analysis of the catalyst bulk structure, ideally considering its entire volume, since the catalyst structure is rarely uniform. Therefore, a single point measurement may not be enough and the application of spatially resolved technique allowing for chemical imaging of the catalyst inside reactor, such as XRD-CT is required ¹⁶. This technique provides physico-chemical insight into a bulk object. Each pixel in the obtained cross section of a bulk object gives chemical information described by a diffraction pattern. Often, interpretation of the diffraction signal from such a pixel may be easier than the overall diffraction pattern obtained by single point measurements. The collected XRD-CT diffraction patterns are obtained via high energy synchrotron radiation and area detectors (enabling fast data acquisition), and can lead to data with a high temporal (20 ms) and spatial resolution (down to 1 μm). Diffraction patterns contain a great number of information, not only about the chemical composition of material but also about the crystallite size or lattice parameter of each component presented in the studied material. Such information can be extracted through the Rietveld analysis and as it was earlier shown by Wragg et al. can be even applied to spatially resolved data ¹⁷.

The main goal of this study is to reveal the solid-state chemistry occurring in the La-Sr/CaO catalyst during temperature ramp in the atmosphere of He and subsequently under OCM reaction conditions. The information about the distribution of each phase inside the whole slice of reactor was obtained by full pattern Rietveld refinement. To our knowledge, this is the first *operando* study reporting on the behaviour of La-Sr/CaO catalytic system under OCM reaction conditions. It reveals the coexistence of two SrCO_3 polymorphs (orthorhombic and rhombohedral) which transform into each other, depending on the reaction conditions (ratio of reagents and GHSV), and thus the temperature of catalyst bed. Two other components present during the OCM reaction: La_2O_3 and mixed CaO-SrO (being mainly CaO) remained stable during the entire duration of the OCM reaction.

2. Experimental Section

2.1 Catalyst synthesis

The preparation of the 10% La₂O₃ -20% SrO /CaO catalyst was performed by impregnating commercial CaCO₃ (>97% purity) as a support using an aqueous solution of La(NO₃)₃ (Sigma Aldrich). After 12 h of drying at 120 °C, it was then promoted with strontium by applying the incipient wetness impregnation of the Sr(NO₃)₂ solution (Sigma Aldrich) followed by 12 h drying at 110 °C. Then the samples were calcined in air for 12 h at 800 °C. Finally, the desired particle size fraction of this catalyst in the range of 200-400 μm was sieved to be used in fixed-bed reactor tests (in laboratory and in ID31 at ESRF).

2.2 Fixed-bed OCM reactor (laboratory tests)

A quartz reactor tube (6 mm external diameter and 4 mm internal diameter) was used to test 60 mg of the catalyst sample. The total flow calculated for two studied values of GHSV 36,000 mL·g⁻¹·h⁻¹ and 72,000 mL·g⁻¹·h⁻¹ were 36 sccm and 72 sccm respectively. Pure gases O₂, CH₄ and N₂ (N₂ as gas dilution for calculating the carbon balance of the GC data) were delivered to the reactor by Bronkhorst mass flow controllers to build 5% nitrogen dilution feed gas in three different methane-to-oxygen ratios (CH₄:O₂ 2:1, 4:1 and 6:1). The catalyst was heated under an atmosphere of N₂ up to 780 °C with a temperature ramp of 10 °C/min, using an electrical tube furnace. The OCM reaction was performed at atmospheric pressure and the outlet gases were analysed by a gas chromatography (Shimadzu) equipped with thermal conductivity detector (TCD) and flame ionization detector (FID).

2.3 *Operando* fixed-bed reactor studies at ID31, ESRF

The catalyst sample of 28 mg was placed inside a quartz tube reactor (external diameter 4 mm, internal diameter 2.5 mm) to form a catalyst bed 8 mm high, supported by glass wool. Pure gases O₂, CH₄ and He were delivered to the reactor by mass flow controllers (Brooks). The

total flow calculated for two studied values of GHSV $36,000 \text{ mL}\cdot\text{g}^{-1}\cdot\text{h}^{-1}$ and $72,000 \text{ mL}\cdot\text{g}^{-1}\cdot\text{h}^{-1}$ were 16.8 sccm and 33.6 sccm respectively. The catalyst was heated under an atmosphere of He (16.8 sccm) up to $780 \text{ }^\circ\text{C}$ with a temperature ramp of $20 \text{ }^\circ\text{C}/\text{min}$, using two air gas heat blowers (Cyberstar). The OCM reaction was performed at atmospheric pressure and the outlet gases were analysed by mass spectrometry using an Ecosys portable mass spectrometer. Two different values of GHSV ($36,000 \text{ mL}\cdot\text{g}^{-1}\cdot\text{h}^{-1}$ and $72,000 \text{ mL}\cdot\text{g}^{-1}\cdot\text{h}^{-1}$) as well as different ratios of CH_4 : O_2 (2:1, 4:1 and 6:1) were tested for the OCM conditions. When changing the CH_4 : O_2 ratio and GHSV the time of 5 minutes was used for the catalyst stabilisation and no data were collected during this period.

2.3.1. Interlaced XRD-CT experiment and data processing

The IXRD-CT experiments were performed at station ID31 at the ESRF using a monochromatic beam of 70 keV with a size of $20 \text{ }\mu\text{m} \times 20 \text{ }\mu\text{m}$. Diffraction patterns were collected using a PILATUS3 X CdTe (Dectris) area detector¹⁸. The catalyst and reactor was mounted on a standard goniometer, placed on a stage allowing for CT movements (rotation and translation of reactor). The photograph of the set up used during this experiment is presented in Figure 1.

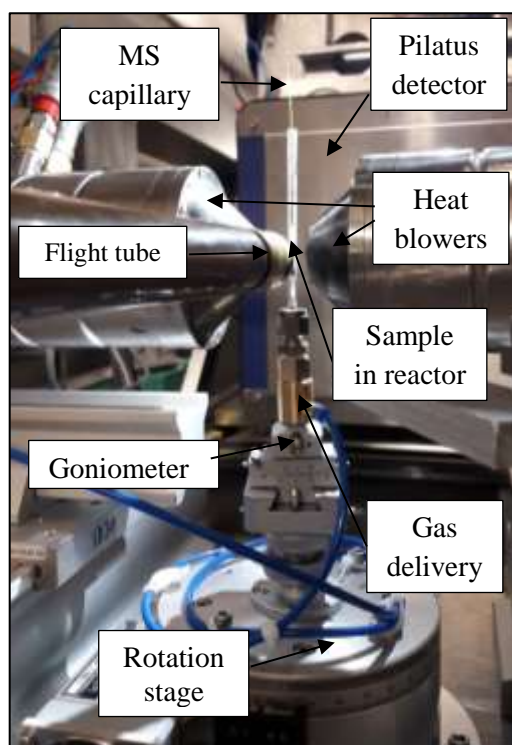


Figure 1. Photograph of the setup used for the experiment at ID31 in ESRF.

The diffraction patterns were collected in Debye-Scherrer geometry, by applying a data collection strategy called interlaced XRD-CT¹⁹. The CT measurements contained 160 angular steps (with angular step size of 1.125°) and 224 translation steps (with translation step equal to the beam size) covering 4.48 mm across the reactor. The obtained reconstructed images of reactor contained 224×224 pixels, with the pixel size of $20 \mu\text{m}$. For the experiment with the interlaced data collection strategy 4 sub-tomo scans were collected, using an angular step of 4.5° for each one. The calibration of detector was performed using a CeO_2 NIST standard. Every 2D diffraction image was converted to 1D powder diffraction pattern using PyFAI software and the image reconstruction was performed using the filtered back projection algorithm in the MATLAB software²⁰⁻²². It is important to note, that the interlaced XRD-CT slices were collected in the middle of catalyst bed.

In order to follow the solid-state changes occurring under *operando* conditions (temperature ramp under He and OCM reaction) time series plots were constructed. Diffraction patterns

collected at a particular angular step (i.e. 224 diffraction patterns for 224 translation steps) were summed and an average diffraction pattern (line scan) was obtained, significantly reducing the number of data to interpret initially. Therefore, the events occurring during the one XRD-CT scan could be described by 160 diffraction patterns (due to the number of angular steps used for the CT scans), with the time resolution of 10 seconds for each line scan. Looking at average diffraction pattern (for each angular step) is a reliable way of investigating the temporal changes. However, one should consider that heterogeneity in the structure, both real and artificial (measurement artefacts) may account for differences in diffraction patterns. Since each pixel in the reconstructed image corresponds to a complete diffraction pattern, as a result 50,000 diffraction patterns were obtained for one XRD-CT measurement. A particular advantage of performing a CT measurement is that it enables spatial separation of the components in the resultant image so that contributions that contribute to the signal 'background' i.e. the glass capillary are essentially removed from the dataset allowing detailed analysis to focus on the evolving solid-state chemistry. However, even after removing the signal 'background' still the number of diffraction patterns coming from the pixels inside the catalytic bed was 10,000. One may find impossible to analyse and treat such high number of data, therefore a special approach leading to the most possibly accurate results in a short time needed to be elaborated.

The obtained chosen diffraction patterns were analysed by X'Pert HighScore Plus software²³ to identify the phases present. Subsequently, Rietveld refinement was performed for the time series of diffraction patterns during the preparation stage (temperature ramp) and OCM conditions (one starting input file for preparation stage and for OCM conditions) using software Topas 5²⁴. The refined parameters of the created model were:

- Lattice parameters (and angle for monoclinic $\text{La}_2\text{O}_2\text{CO}_3$ phase),
- Scale factors,

- Crystallite size (Lorentzian) with the size being constrained between 20 and 500 nm,
- Isotropic temperature factors constrained between 0.1 and 5 for lower temperature (below 600 °C) and 0.1 and 10 for higher temperatures (above 600 °C). Isotropic temperature factors for each atom inside one structure were set to be equal, in order to decrease the number of parameters to refine.
- Occupancy of Ca²⁺ atom constrained between 0 and 1 in the Ca_xSr_{1-x}O oxide. The occupancy of Sr²⁺ was calculated by the equation 1-X_{Ca}.
- Background coefficients (10th degree order Chebyshev polynomial).

After creating two input files, accurately representing all phases present during the temperature ramp or OCM reaction respectively, they were used for the refinement of each diffraction pattern in time series or in reconstructed image. An in-house MATLAB script was developed in order to create the input file for batch refinement, which was subsequently sent to TOPAS 5 for refinement and the obtained results for the refined chosen parameters could be plotted as a function of time (in time series) or as a map (for space resolved data). Depending on the number of parameters and complexity of refinement, entire XRD-CT reconstructed image could be refined in around 4h time.

Results and discussion

3.1 Preparation stage

For an easier explanation of how the chemistry evolves inside the catalytic bed during the preparation stage (temperature ramp under He) the section was divided into three parts. Each of them presents the evolution of the compounds containing the principal elements lanthanum, strontium and calcium respectively. The weight percent corresponds to total composition of catalyst and was calculated with Topas software ²⁴. A detailed review of previously reported solid-state transformation events for the components presented in the La-Sr/CaO catalyst,

induced by temperature is presented in the supporting information. Tables presenting the different identified phases together with the crystallographic details can be also found in the supporting information.

3.1.1 Lanthanum containing phases

Figure 2 shows the weight percent changes as a function of temperature (from room temperature to 780 °C) under He for components containing lanthanum in their structure.

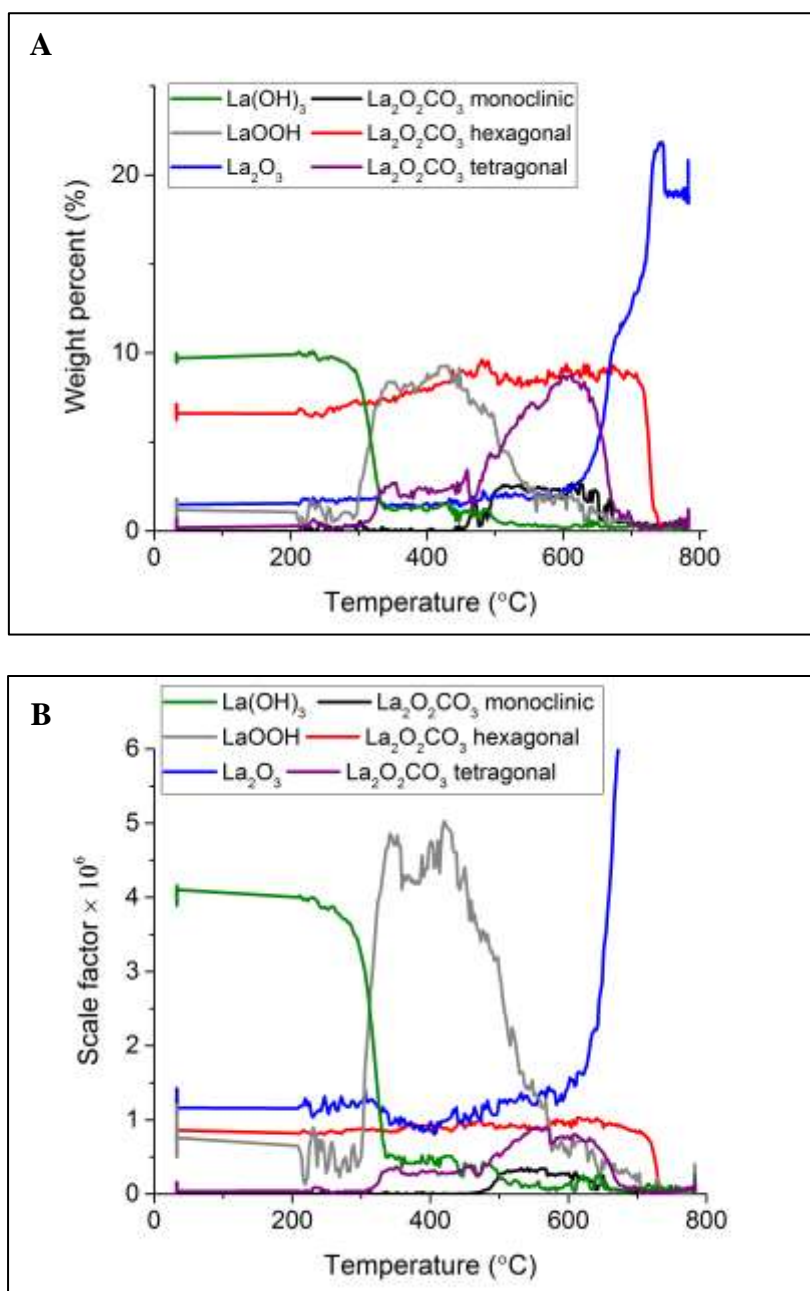
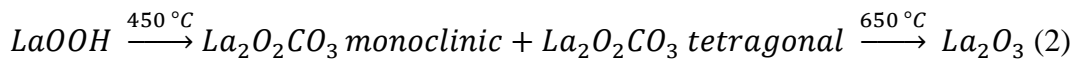
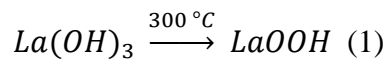


Figure 2. Panel A: Weight percent composition of crystalline lanthanum containing phases and panel B: scale factors of crystalline lanthanum containing phases as a function of temperature during temperature ramping under He to 780 °C.

The starting material consisted mainly of La(OH)₃ (10 %) and hexagonal La₂O₂CO₃ (6 %); the remaining 3% comprised La₂O₃. During the temperature ramp, the first observed change is the decomposition of hexagonal La(OH)₃ into monoclinic LaOOH around 300 °C. The formed monoclinic LaOOH disappeared around 450 °C and two other polymorphs of La₂O₂CO₃ monoclinic and tetragonal (with the majority of tetragonal) were formed from the LaOOH. The high weight percent of formed tetragonal polymorph of La₂O₂CO₃ (around 8 %) was possibly caused by CO₂ adsorbed on the catalyst, since there was no additional source of CO₂ at this stage of temperature ramp. Subsequently, monoclinic and tetragonal phases disappeared around 650 °C which lead to formation of hexagonal La₂O₃. The hexagonal La₂O₂CO₃ was consumed at 750 °C. When reaching 780 °C hexagonal La₂O₃ was the only phase present coming predominantly from the decomposition of all present La₂O₂CO₃. A summary of the proposed lanthanum solid-state chemistry evolution inside the reactor during the temperature ramp under He is given below:



The decomposition of La(OH)₃ to LaOOH at 300 °C is consistent with the results of study performed by Yamamoto et al. and Fleming et al.^{25 26}. As reported by Wang et al. and Chen et al. it is possible to obtain La₂O₂CO₃ (hexagonal or monoclinic) from La(OH)₃ by calcination at high temperature (400 – 500 °C)^{27 28}. The subsequent decomposition temperature of LaOOH

derived from this study is also consistent with results reported by Fleming et al. and Schafer and Roy, however, the products which were formed are different; La_2O_3 as a product was reported in their study, whereas in this experiment two polymorphs of $\text{La}_2\text{O}_2\text{CO}_3$ were found^{26 29}. The three-step decomposition of $\text{La}(\text{OH})_3$, proposed by Yamamoto did not occur during heating in He, which can be confirmed by the results of mass spectrometry performed (see Figure 6 in subsequent section)²⁵. Finally, the decomposition of $\text{La}_2\text{O}_2\text{CO}_3$ is consistent with observations previously reported by Shirsat et al.³⁰.

3.1.2 Calcium containing phases

Figure 3 shows the weight percent changes as a function of temperature (from room temperature to 780 °C) under He for components containing calcium in their structure.

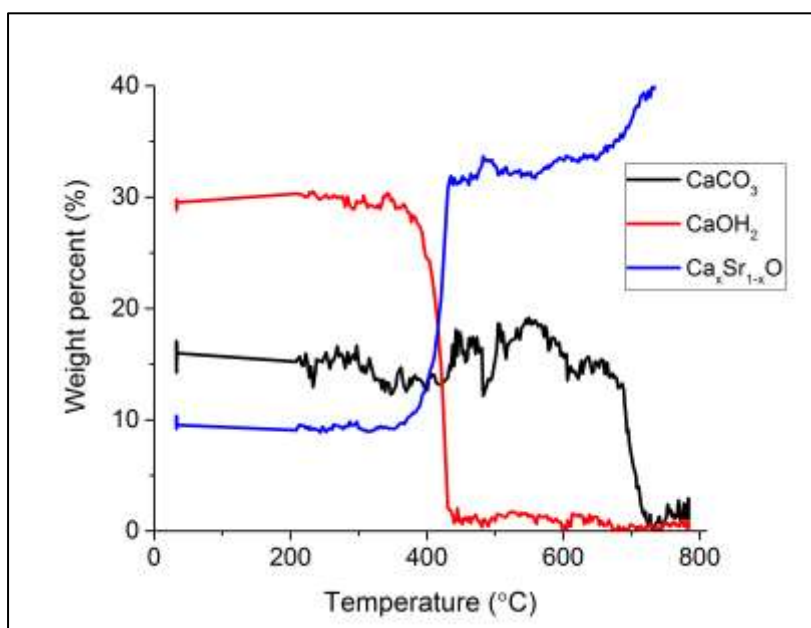
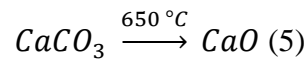
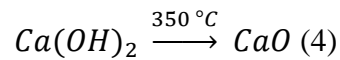


Figure 3. Weight percent changes of components containing calcium as a function of temperature during the preparation stage under He.

The starting catalyst material consisted of hexagonal $\text{Ca}(\text{OH})_2$ (30 %) rhombohedral CaCO_3 (15 %) and cubic CaO-SrO mixed oxide (10 %). The $\text{Ca}(\text{OH})_2$ disappeared at around 350 °C

and this simultaneously lead to formation of $\text{Ca}_x\text{Sr}_{1-x}\text{O}$. The further increase in temperature lead to decomposition of CaCO_3 at 650 °C to form the mixed CaO-SrO oxide. Through the remainder of the preparation stage, the mixed oxide contained mainly CaO (average occupancy of Ca^{2+} in mixed oxide was 0.99).

The proposed path of solid-state evolution of calcium containing compounds inside the reactor during the temperature ramp under He is observed as follows:



The observed events during the preparation stage confirmed what was reported previously. Beruto et al. found that Ca(OH)_2 decomposed to CaO at 320 °C while the CaCO_3 decomposed to CaO at 510 °C ³¹. In addition, another study reported that the temperature of Ca(OH)_2 decomposition was 460 °C, whereas the temperature of CaCO_3 decomposition was 650 °C ³². The miscibility between CaO and SrO oxides was studied by Jacob et al. ³³. They reported the formation of different pseudo- binary solutions between CaO and SrO from CaCO_3 and SrCO_3 by ball milling and decomposition of carbonates under vacuum in 800 °C. During this study, the slight decrease in the occupancy of Ca atoms, which corresponded to substitution of Ca^{2+} by Sr^{2+} in the mixed oxide CaO-SrO started at the temperature of 750 °C, however, during the entire temperature ramp the occupancy of Ca^{2+} remained very high (on average 0.99) and the mixed oxide was mainly CaO phase.

3.1.3. Strontium containing phases

Figure 4 shows the weight percent changes as a function of temperature (from room temperature to 780 °C) under He for components containing strontium in their structure.

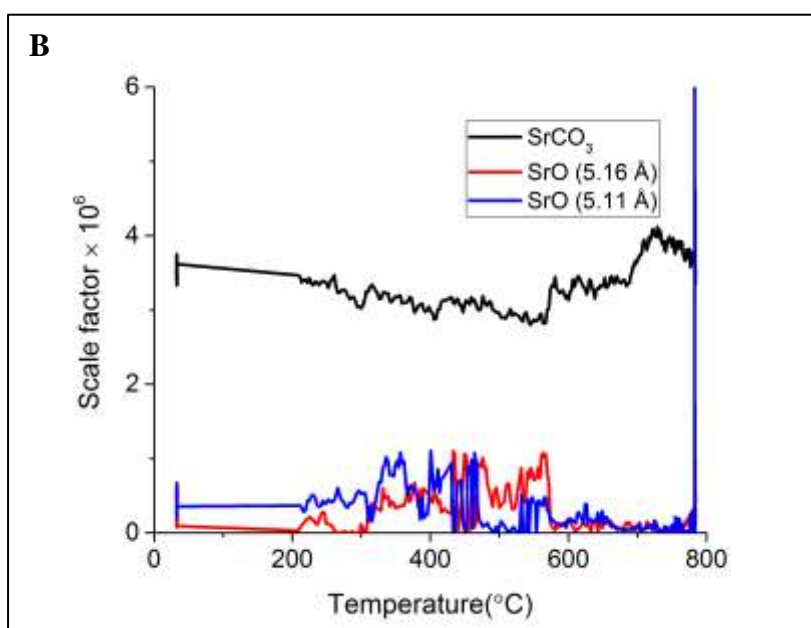
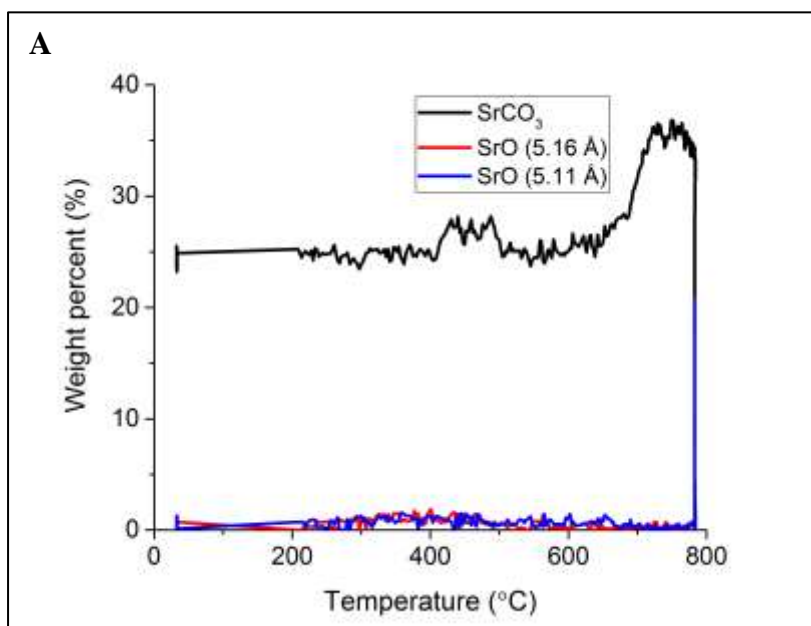


Figure 4. Panel A: Weight percent composition of crystalline strontium containing phases and panel B: scale factors of crystalline strontium containing phases as a function of temperature during temperature ramping under He to 780°C.

The starting catalyst material contained orthorhombic SrCO₃ (25 %), which remained stable up to 650 °C. Then its quantity was increased, which according to the results obtained from the Rietveld refinement from the Figure 4A does not result from the decomposition of any other

phase containing strontium. This may be explained by the change in mass of catalyst during the temperature ramp, as previously observed for lanthanum containing phases, since the scale factor of SrCO₃ remained stable (Figure 4B). At 750 °C the orthorhombic SrCO₃ decomposed into two cubic SrO oxides, which could be spatially distinguished due to a difference in the size of their lattice parameter: 5.11 Å vs 5.16 Å (their weight percent was 8% and 19% respectively). The spatial distribution of these two phases is presented in Figure 5. The coexistence of the same cubic SrO phase with two different lattice parameter size may have resulted as a consequence of different solid-state reactions (exothermic/endothermic) occurring inside the reactor during the temperature ramp. At the same time, there may existed a chemical difference between these two SrO phases, however such information could not be verified by Rietveld analysis.

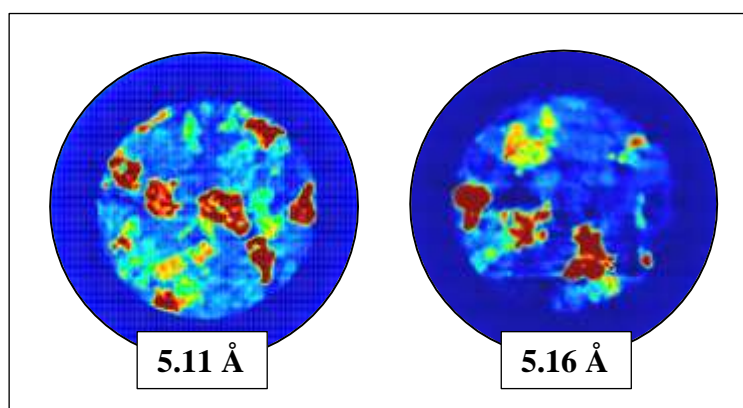
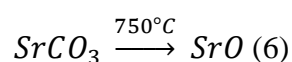


Figure 5. Spatial distribution of two different SrO cubic phases, with different lattice parameter. The XRD-CT scan was collected at 780 °C in He.

The proposed path of different events occurring inside the reactor during the temperature ramp under He regarding the components containing strontium is observed as follows:



The observed decomposition temperature of SrCO₃ at 750 °C is in agreement with the reported literature³⁴. As observed by Iwafuchi et al. decomposition temperature of SrCO₃ was strongly dependent on atmosphere in which the sample was placed (partial pressure of CO₂)³⁵. SrCO₃ can decompose in temperatures lower than its transition in the flow of pure N₂. No phase transition from orthorhombic SrCO₃ to rhombohedral SrCO₃ was observed during the preparation stage of catalyst, thus SrCO₃ decomposed before the temperature necessary for the phase transition was reached³⁶.

3.1.4 Online mass spectrometry analysis

Results of mass spectrometry confirmed the observed events taking place during the preparation stage. The first broad peak of H₂O could be observed between 150 °C and 250 °C, which corresponds to the desorption of water from the catalyst surface. The second peak could be observed in the temperature range between 300 °C and 500 °C and can be attributed to the decompositions of La(OH)₃, LaOOH and Ca(OH)₂. As it is shown on Figure 6, several short periods could be distinguished during this event, which may result from the complexity of the decomposition process. It is probable that due to the uneven temperature distribution across the reactor and along the catalyst bed, different components decomposed at different times. As for CO₂, two broad peaks can be observed. The first is observed between 600 °C and 780 °C and corresponds to the decomposition of La₂O₂CO₃ (all three polymorphs), CaCO₃ and SrCO₃ whereas the second peak at 780 °C corresponds to the further decomposition of SrCO₃.

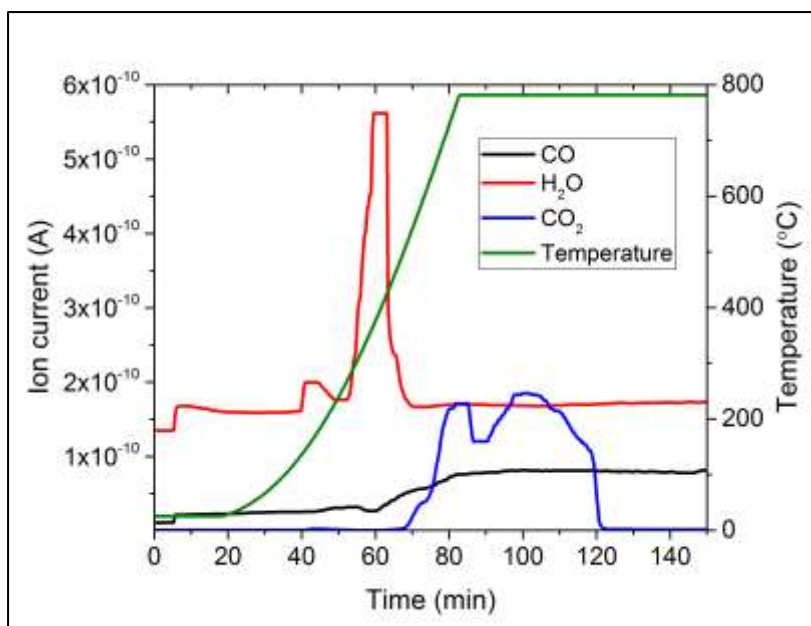


Figure 6. Mass spectrometry results collected during the preparation stage of La-Sr/CaO catalyst under He with the corresponding temperature axis.

3.2 Oxidative coupling of methane

Table 1. Identified phases of La-Sr/CaO catalyst during the OCM conditions.

Phase	Crystallographic details	ICSD database code	Lattice parameter (Å)
SrCO ₃	Orthorhombic, Pmcn	15195	$a = 5.138$ $b = 8.516$ $c = 6.307$
SrCO ₃	Rhombohedral, R-3mH	27445	$a = 5.104$ $c = 9.452$
Ca _x Sr _{1-x} O	Cubic, Fm-3m	04-006-6637 (PDF number)	$a = 4.888$
La ₂ O ₃	Hexagonal, P63/mmc	100208	$a = 3.982$ $c = 6.234$
CaCO ₃	Rhombohedral, R-3c	40114	$a = 4.899$ $c = 16.038$
La-SrO	Monoclinic, C1c1	16357	$a = 11.854$

			$b = 7.371$ $c = 13.342$ $\beta = 116.39^\circ$
--	--	--	---

Table 1 presents the identified phases during the OCM reaction conditions in the structure of the La-Sr/CaO catalyst. Figure 7 shows the weight percent changes during the OCM reaction conditions obtained for the Rietveld refinement of time series. Note that between changing CH₄: O₂ ratio and GHSV there was a period of 5 minutes where data were not collected (catalyst stabilisation period).

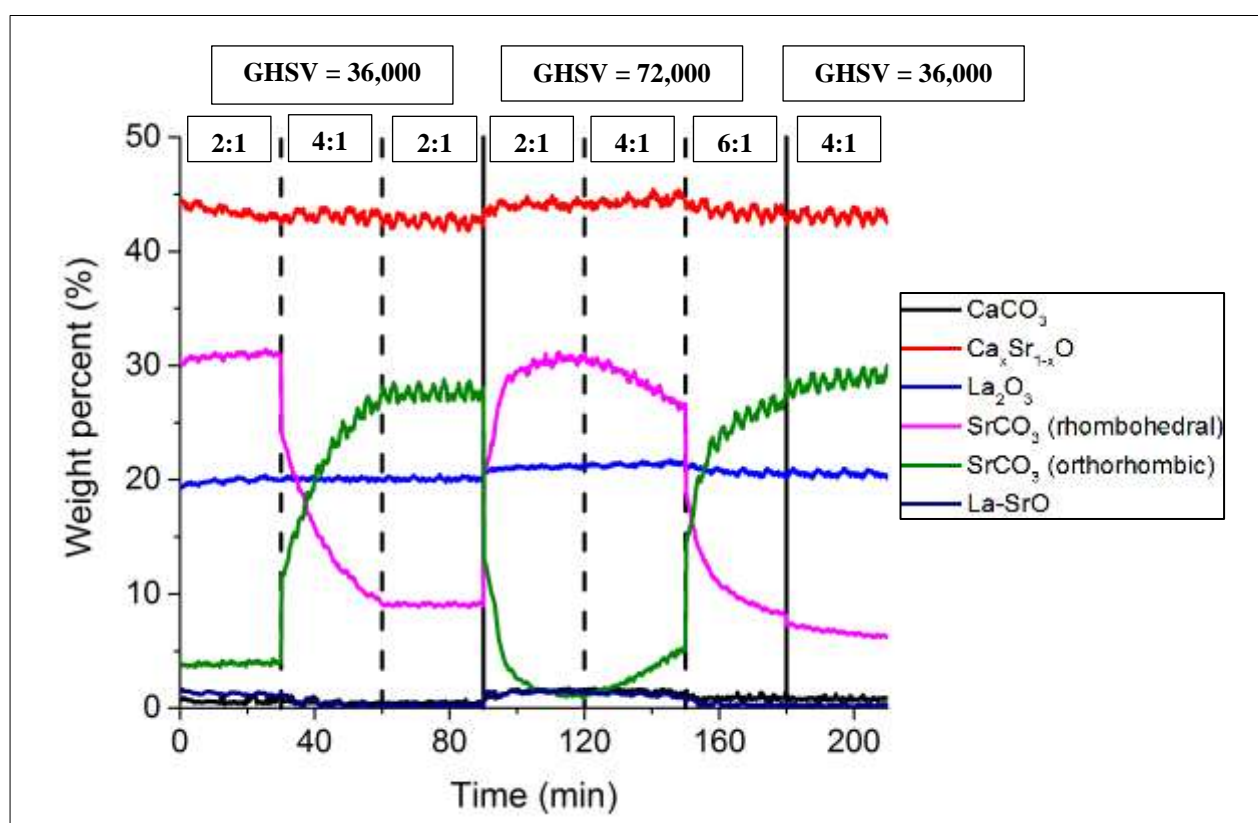


Figure 7. Results of the Rietveld refinement of time resolved data collected under *operando* conditions during the OCM reaction. Tabulated results of the weight percent are provided in the supporting information.

The most significant solid-state change taking place under OCM reaction conditions was related to phase transition between rhombohedral (higher temperature polymorph) and

orthorhombic (lower temperature polymorph) SrCO₃. The SrCO₃ phase was reformed due to the reaction between SrO, present at the final state of catalyst at high temperature, and CO₂ formed during the reaction. High partial pressure of CO₂ led to this transition, before the decomposition of SrCO₃³⁵. The two SrCO₃ phases seemed to present a cyclic behaviour during the OCM experiment. Transition between orthorhombic and rhombohedral SrCO₃ is reversible and as reported previously occurs around 920 °C, depending on carbonates composition (presence of Ba) or atmosphere in which sample was present (presence of CO₂)³⁶. Orthorhombic – rhombohedral transition for the isomorphous structure BaCO₃ was found to occur at 811 °C³⁷. Zhang et al. also observed the SrCO₃ transition (in the mixture with BaCO₃) from orthorhombic to rhombohedral at 700 °C by performing *in situ* XRD³⁸. However, no transformation to cubic SrCO₃ was observed during this experiment³⁸. Results of Rietveld-CT refinement also confirmed this transition (Figure 8). However, since temperature was not monitored during the OCM reaction, it is not possible to state the exact temperature of this transition during our experiment. The results of Rietveld refinement for all the other phases can be found in the supporting information (first and last XRD-CT scan of OCM reaction).

All the other components seemed to not undergo any changes during the OCM reaction. The contribution of the CaCO₃ and mixed oxide of La-SrO was little and considering the error on the estimated weigh percent from the Rietveld refinement, their presence may be questionable. However, the value of R_{wp} and GOF (goodness of fit) were better when the model accounted for these two phases (R_{wp} = 3.84 and GOF 1.59 for model with CaCO₃ and La-SrO phases; R_{wp} = 4.02 and GOF 1.66 for model without CaCO₃ and La-SrO phases).

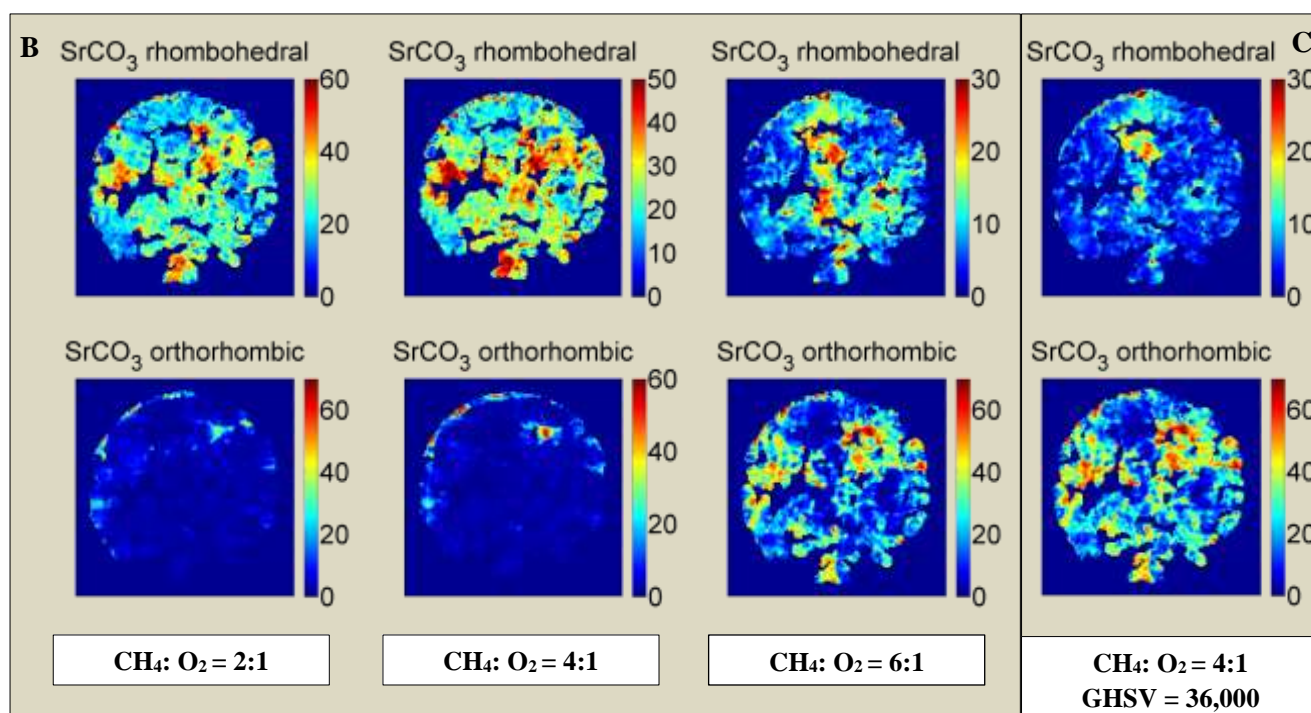
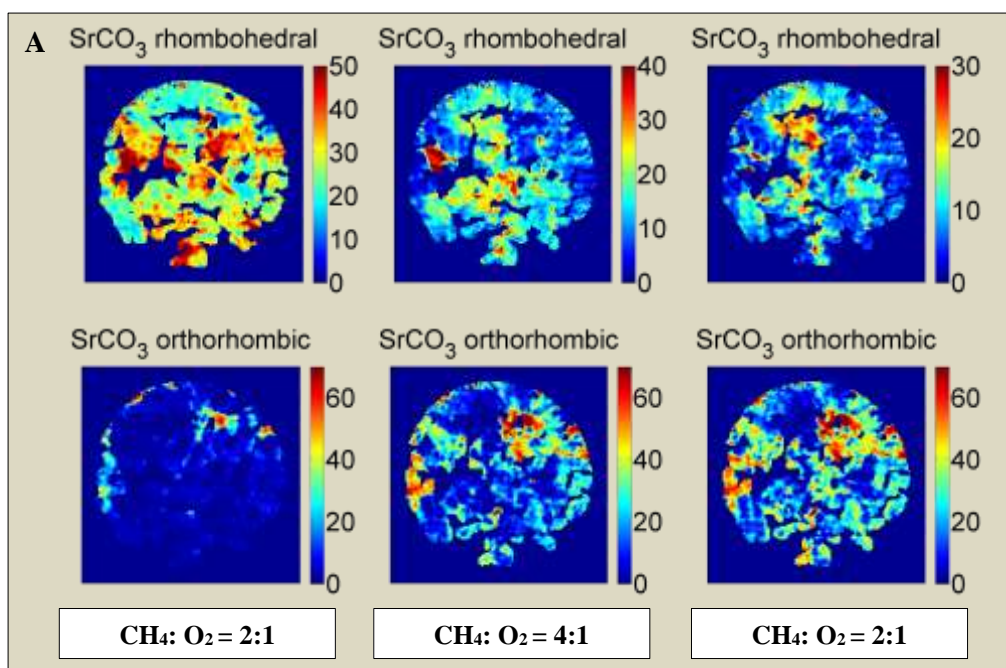
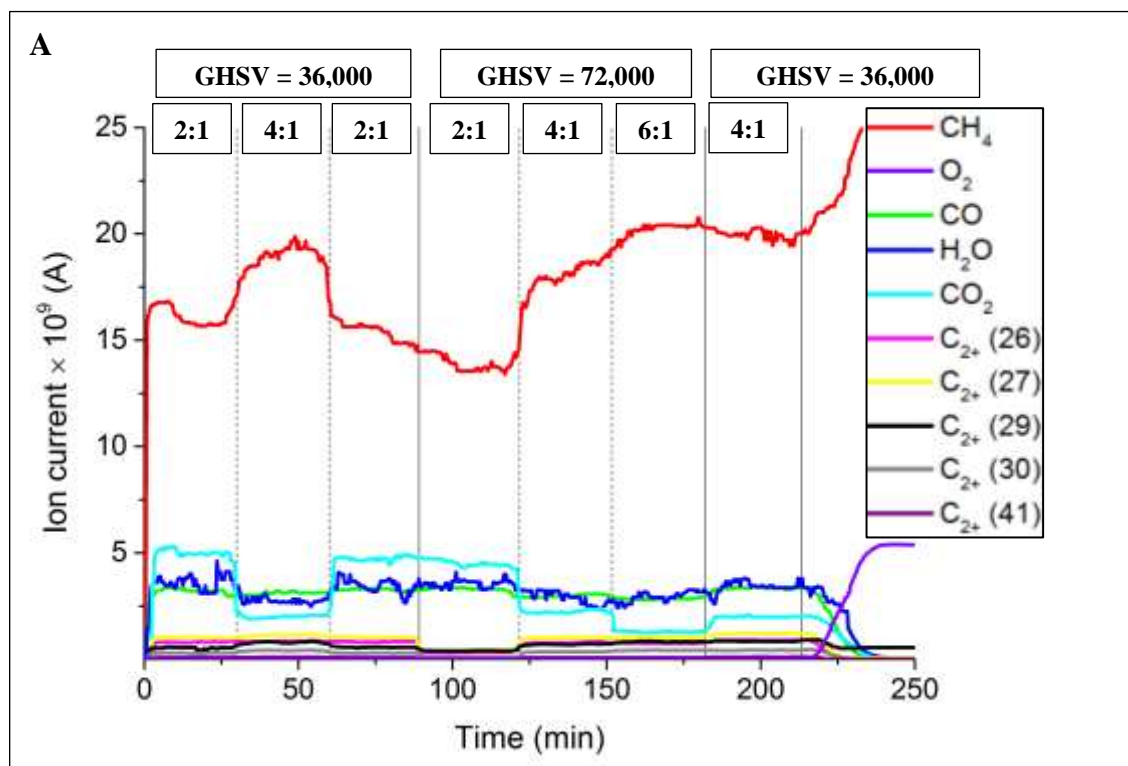


Figure 8. Results of Rietveld-CT refinement for the OCM conditions presenting the weight percent spatial distribution: panel A – GHSV 36,000 mL·g⁻¹·h⁻¹, panel B - GHSV 72,000 mL·g⁻¹·h⁻¹ and panel C – GHSV 36,000 mL·g⁻¹·h⁻¹ (the last XRD-CT scan).

From Figure 8A it can be observed that the orthorhombic SrCO₃ was formed in the same region where previously the SrCO₃ rhombohedral was present. This growth occurred during the second XRD-CT scan (for CH₄: O₂ being 4:1) and was sustained during the third XRD-CT scan with CH₄: O₂ being 2:1. Then the GHSV was doubled and the rhombohedral SrCO₃ was reproduced in the same region where it previously existed (during the first XRD-CT scan under OCM reaction conditions), which confirmed the cyclic behaviour of the SrCO₃ polymorphs. We note that in both Figures 8A and 8B increasing CH₄: O₂ saw an increase in the amount of the orthorhombic polymorph (and subsequent decrease in the amount of rhombohedral polymorph) which was initially located as a semi-circular/three-quarter contiguous ring at the periphery of the reactor, spreading further into the middle of the reactor with higher O₂ content in the reactor feed.

3.2.1. Online mass spectrometry data



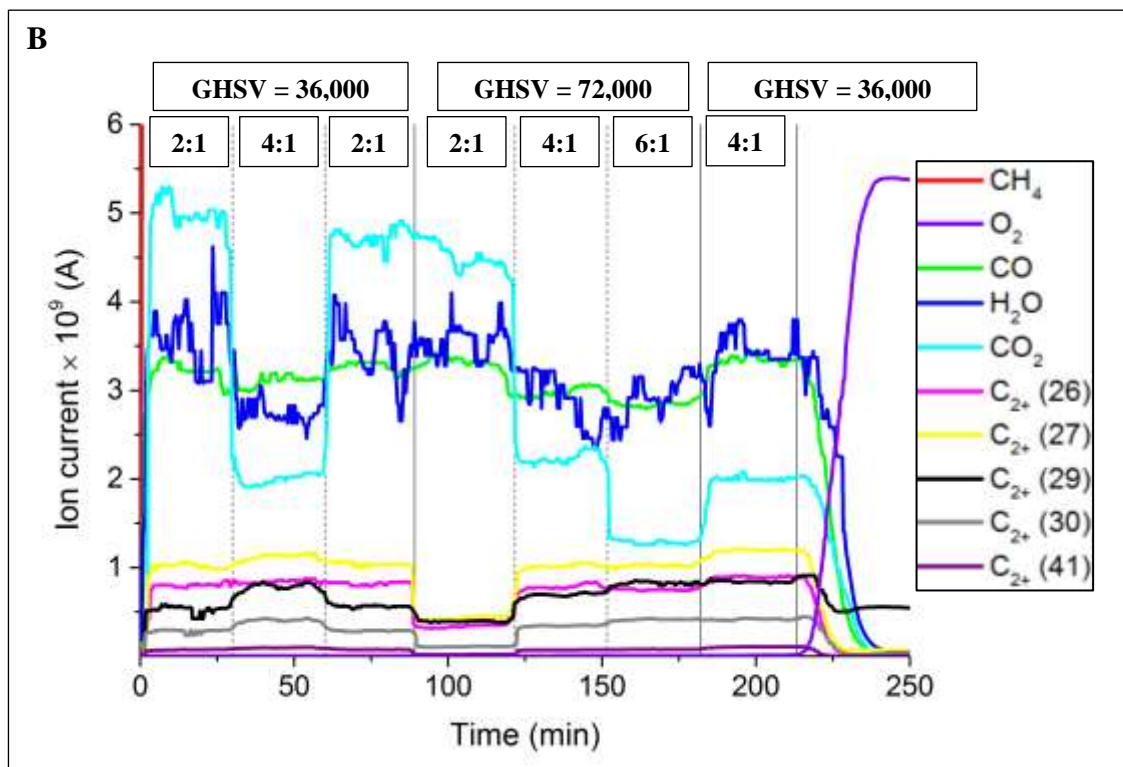


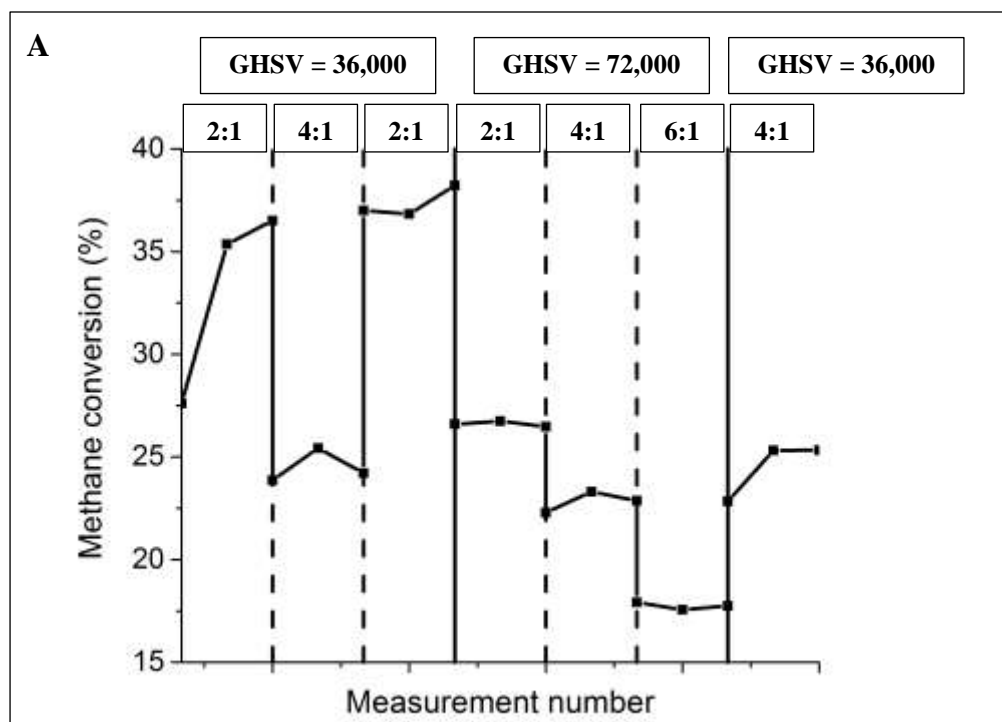
Figure 9. Mass spectrometry results (panel A), and the zoomed region of interest (panel B) presenting the C_{2+} production (from the beginning of the OCM reaction).

Figure 9A presents the results obtained from the mass spectrometry measurements collected during the OCM experiment while the region of interest (production of C_{2+} molecules) is presented on the Figure 9B. The results of mass spectrometry presented here have only qualitative character. Note that, the sampling volume used for the mass spectrometry detection stayed constant during the experiment and therefore only changes in the products or reagents ratio detected can be actually observed. Therefore, no signal change, when doubling the GHSV could be observed for the CH_4 for the same $CH_4: O_2$ ration, unless a change in the CH_4 conversion occurred during the reaction.

As it can be observed, the production of C_{2+} molecules was mainly correlated with the conditions applied during the OCM process ($CH_4: O_2$ ratio and GHSV). The highest production

of CO₂ was observed when 2:1 ratio of CH₄: O₂ was used and decreasing of this ratio to 4:1 and then 6:1 led to lower production of CO₂. The production of CO seemed to follow the same trend as CO₂, however the change in the response of the mass spectrometry signal was very small. The highest production of C₂H₄ (m/z = 26 and m/z = 27) was found for 4:1 CH₄: O₂. When the GHSV was double, the production of C₂₊ molecules dropped down. The higher GHSV resulted in higher total flow of reagents and lower contact time between the catalyst and reagents. Therefore, the production of C₂₊ molecules and CO₂ was expected to be lower. Decreased selectivity for C₂₊ molecule production could be observed with higher O₂ concentrations³⁹. When increasing the CH₄: O₂ ratio, the selectivity for desired products could be enhanced, but the CH₄ conversion was decreased. Since the conversion of CH₄ depends on the CH₄: O₂ ratio, the highest methane conversion was obtained for 2:1 CH₄: O₂. It is important to note that the colour of catalyst did not change after the experiment (remained white), suggesting that no formation of carbon occurred during the OCM reaction.

3.4 Fixed-bed reactor laboratory tests



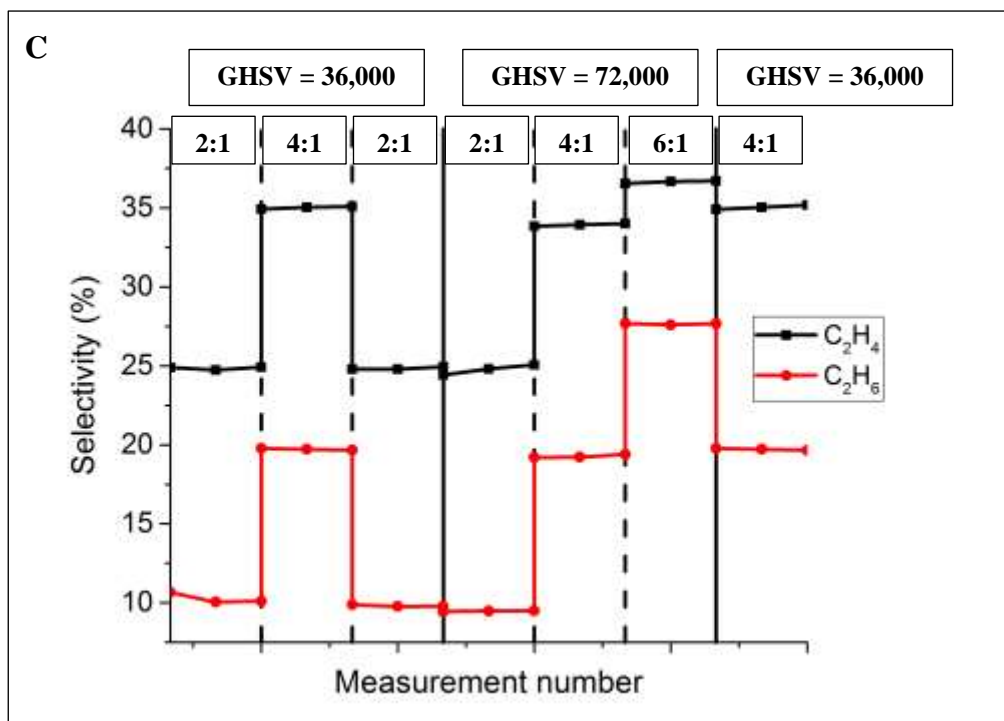
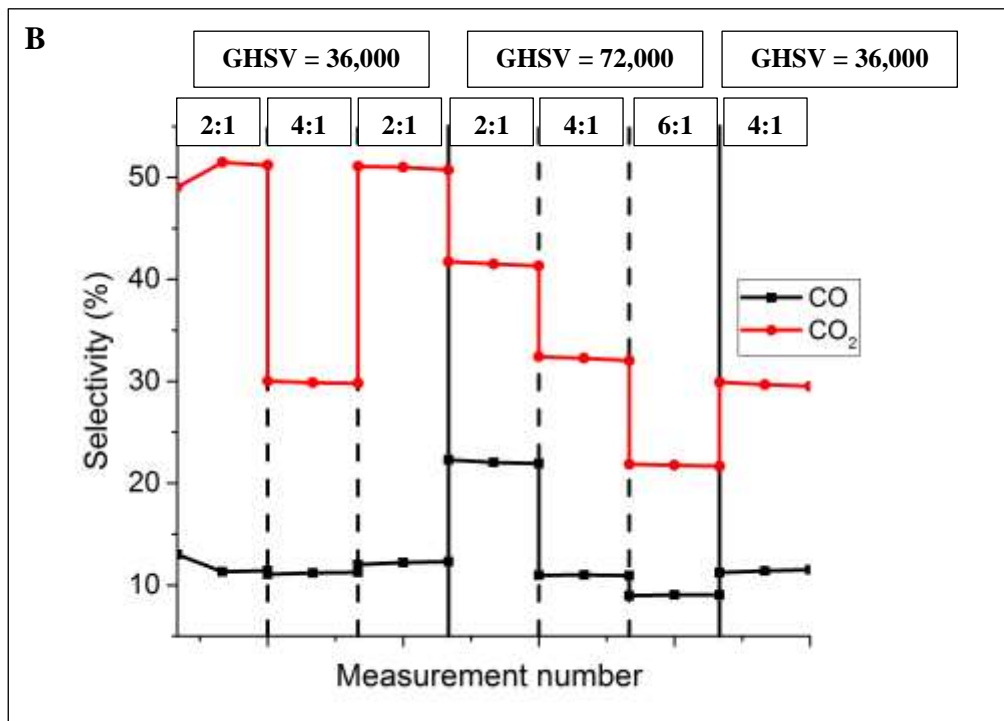


Figure 10. Panel A: methane conversion, panel B: selectivity for CO₂ and CO and panel C: selectivity for C₂H₄ and C₂H₆ during the OCM reaction under different conditions (CH₄: O₂

and GHSV). Tabulated results of the OCM experiment (conversion, selectivity and yield) can be found in the supporting information.

Figure 10 presents the results from the OCM reaction experiment performed in the laboratory using a fixed-bed reactor. As it can be observed from the reported results, the CH₄ conversion depended on the CH₄: O₂ ratio introduced to process; it decreased when CH₄: O₂ ratio increased. In the same time, the selectivity for C₂H₆ increased while the selectivity for CO₂ decreased. Selectivity of CO seemed to be rather stable through the entire duration of experiment and oscillated between 13% and 18%. Selectivity for C₂H₄ gradually increased for the GHSV = 36,000. However, for the CH₄: O₂ ratio equal to 6:1 and GHSV equal to 72,000 mL·g⁻¹·h⁻¹ selectivity for C₂H₄ significantly decreased. Overall, the selectivity for C₂H₄ was between 21-31 % with the C₂H₄ yield between 6.7 – 9.3 %. The ratio between yields of C₂H₄ and C₂H₆ depends on the CH₄: O₂ used; the highest ratio of 2.4 could be obtained for CH₄: O₂ ratio equal to 2:1 and GHSV 72,000 mL·g⁻¹·h⁻¹.

Results obtained from *operando* measurements with mass spectrometry showed excellent agreement with the catalytic results obtained in the laboratory fixed-bed reactor. In experiments where either the CH₄: O₂ ratio was comparatively low (i.e. 2:1) or else the GHSV was low, CH₄ conversion and CO₂ selectivity were comparatively high; this was also coincident with the reappearance (as observed by XRD-CT) of the high temperature polymorph of SrCO₃ (Figure 9B), which, we rationalise, was driven by the increase in temperature of the catalyst bed due to dominance of hydrocarbon combustion over the less exothermic OCM reaction⁴⁰. No other obvious changes in the XRD data were observed.

Summary and conclusion

We presented the first *operando* study of OCM process, with La-Sr/CaO catalyst, using interlaced XRD-CT technique. Each pixel of the reconstructed XRD-CT image, leading to a

complete diffraction pattern, was used to obtain the weight percentage map of each component inside the cross section of the reactor. High temporal resolution between collected diffraction patterns (~ 10 seconds) enabled us to follow the different processes of formation and decomposition during the catalyst preparation stage – temperature ramp and OCM reaction. By performing an imaging study, a more representative overview of phase evolution inside the reactor was obtained.

The results collected during the OCM reaction showed the presence of La_2O_3 and CaO-SrO which remained comparatively stable during the entire reaction time whereas a temperature-driven cyclic behaviour between two polymorphs of SrCO_3 (rhombohedral-orthorhombic), was observed. During the OCM reaction, at the point of measurement, the temperature of catalyst bed gradually decreased (due to higher rate of relatively less exothermic yet more desirable reaction such as OCM), which could be deduced from the behaviour of these two polymorphs; i.e. a greater presence of the lower temperature orthorhombic SrCO_3 polymorph. Once the GHSV was doubled and/or the O_2 : CH_4 ratio increased, combustion reactions begin to dominate and therefore the temperature of the catalyst bed at the point of measurement increased; inferred by the reformation of higher temperature polymorph of SrCO_3 (rhombohedral). Since measurements were performed in the middle of the reactor, it is not possible to say whether the same temperature variation with gas composition/space velocity is seen over the remainder of the catalyst bed. As has been shown previously however, parameters such as flow rate and reactant composition can lead to temperature/reaction gradients along the length of a reactor bed and that measurement at a different height (particularly further along the catalyst bed when operating at higher space velocities) in the sample may result in differing amounts of the SrCO_3 polymorph to that observed in the middle of the reactor bed ⁴¹. By examining a number of reaction conditions in this study however, it is clear that the solid-state chemistry of the other compounds is very unlikely to be affected by the sample height measurement.

Since catalysis is a surface phenomenon and that the formation of the desired C₂ products in the OCM reaction is thought to occur via reaction in the gas-phase the results of catalytic studies cannot be fully correlated with the evolution of crystalline phases present in the catalyst under reaction conditions, particularly when using a bulk sensitive technique such as XRD⁴². However, full profile analysis of XRD-CT data did allow for identifying presence of SrCO₃ polymorphs and the mapping of their spatial distribution. Working on the basis that the presence of the rhombohedral polymorph is caused by higher temperatures, it is then possible to state that in the first instance we were able to observe temperature gradients in the catalyst bed on a pixel-by-pixel basis and furthermore this can be rationalised by the type of catalytic reaction taking place (i.e. combustion vs. OCM). Although extraction of information regarding sample temperature from XRD-CT has previously been shown by some of us, it was only possible to demonstrate that sample heating was uniform⁴³. Clearly then these results show that in addition to the large amount of information concerning solid-state phase evolution there is also potential for this *operando* XRD-CT approach to observe and put into context temperature/reactivity gradients thereby allowing a more comprehensive evaluation of the performance of catalytic and/or other functional materials under reaction conditions.

Acknowledgement



This project has received funding from the European Union's Horizon 2020 research and innovation programme under grant agreement No 679933 (MEMERE project).

Supporting Information

Review of previously reported solid-state transformation events for the components presented in the La-Sr/CaO catalyst. Crystallographic information on identified phases during the preparation stage. Weight percent changes and temperature ramp as a function of number of

scan during the preparation stage. Rietveld refinement results plots during the preparation stage and the OCM reaction. Rietveld refinement-CT results during the OCM reaction (first and last XRD-CT scan). Weight percent composition during the OCM reaction. Tabulated results of laboratory fix-bed OCM experiment.

References

- (1) Keller, G. E.; Bhasin, M. M. Synthesis of Ethylene via Oxidative Coupling of Methane I. Determination of Active Catalysts. *J. Catal.* **1982**, *73*, 9–19.
- (2) Cueto-Felgueroso, L.; Juanes, R. Forecasting Long-Term Gas Production from Shale. *Proc. Natl. Acad. Sci.* **2013**, *110*, 19660–19661.
- (3) Godini, H. R.; Xiao, S.; Jašo, S.; Stünkel, S.; Salerno, D.; Son, N. X.; Song, S.; Wozny, G. Techno-Economic Analysis of Integrating the Methane Oxidative Coupling and Methane Reforming Processes. *Fuel Process. Technol.* **2013**, *106*, 684–694.
- (4) Olivier, L.; Haag, S.; Pennemann, H.; Hofmann, C.; Mirodatos, C.; van Veen, A. C. High-Temperature Parallel Screening of Catalysts for the Oxidative Coupling of Methane. *Catal. Today* **2008**, *137*, 80–89.
- (5) Wang, J.; Chou, L.; Zhang, B.; Song, H.; Zhao, J.; Yang, J.; Li, S. Comparative Study on Oxidation of Methane to Ethane and Ethylene over Na₂WO₄-Mn/SiO₂ Catalysts Prepared by Different Methods. *J. Mol. Catal. A Chem.* **2006**, *245*, 272–277.
- (6) Zeng, Y.; Lin, Y. S. Catalytic Properties of Yttria Doped Bismuth Oxide Ceramics for Oxidative Coupling of Methane. *Appl. Catal. A, Gen.* **1997**, *159*, 101–117.
- (7) Choudhary, V. R.; Uphade, B. S.; Mulla, S. A. R. Oxidative Coupling of Methane over a Sr-Promoted La₂O₃ Catalyst Supported on a Low Surface Area Porous Catalyst Carrier. *Ind. Eng. Chem. Res.* **1997**, *36*, 3594–3601.

- (8) Imanaka, N.; Masui, T.; Kato, Y. Preparation of the Cubic-Type La_2O_3 Phase by Thermal Decomposition of LaI_3 . *J. Solid State Chem.* **2005**, *178*, 395–398.
- (9) Conway, S. J.; Greig, J. A.; Thomas, G. M. Comparison of Lanthanum Oxide and Strontium-Modified Lanthanum Oxide Catalysts for the Oxidative Coupling of Methane. *Appl. Catal. A, Gen.* **1992**, *86*, 199–212.
- (10) Granados, M. L.; Poves, M. D. Z.; Alonso, D. M.; Mariscal, R.; Galisteo, F. C.; Moreno-Tost, R.; Santamaría, J.; Fierro, J. L. G. Biodiesel from Sunflower Oil by Using Activated Calcium Oxide. *Appl. Catal. B Environ.* **2007**, *73*, 317–326.
- (11) Beck, B.; Fleischer, V.; Arndt, S.; Hevia, M. G.; Urakawa, A.; Hugo, P.; Schomäcker, R. Oxidative Coupling of Methane-A Complex Surface/gas Phase Mechanism with Strong Impact on the Reaction Engineering. *Catal. Today* **2014**, *228*, 212–218.
- (12) Taylor, R. P.; Schrader, G. L. Lanthanum Catalysts for Methane Oxidative Coupling: A Comparison of the Reactivity of Phases. *Ind. Eng. Chem. Res.* **1991**, *30*, 1016–1023.
- (13) Vamvakeros, A.; Jacques, S. D. M.; Middelkoop, V.; Di Michiel, M.; Egan, C. K.; Ismagilov, I. Z.; Vaughan, G. B. M.; Gallucci, F.; van Sint Annaland, M.; Shearing, P. R.; et al. Real Time Chemical Imaging of a Working Catalytic Membrane Reactor during Oxidative Coupling of Methane. *Chem. Commun.* **2015**, *51*, 12752–12755.
- (14) Bhatia, S.; Thien, C. Y.; Mohamed, A. R. Oxidative Coupling of Methane (OCM) in a Catalytic Membrane Reactor and Comparison of Its Performance with Other Catalytic Reactors. *Chem. Eng. J.* **2009**, *148*, 525–532.
- (15) Beale, A. M.; Jacques, S. D. M.; Weckhuysen, B. M. In-Situ Characterization of Heterogeneous Catalysts Themed Issue Chemical Imaging of Catalytic Solids with Synchrotron Radiation. *Chem. Soc. Rev.* **2010**, *39*, 4656–4672.
- (16) Jacques, S. D. M.; Di Michiel, M.; Beale, A. M.; Sochi, T.; O'Brien, M. G.; Espinosa-

- Alonso, L.; Weckhuysen, B. M.; Barnes, P. Dynamic X-Ray Diffraction Computed Tomography Reveals Real-Time Insight into Catalyst Active Phase Evolution. *Angew. Chemie Int. Ed.* **2011**, *50*, 10148–10152.
- (17) Wragg, D. S.; O'Brien, M. G.; Di Michiel, M.; Lonstad-Bleken, F. Rietveld Analysis of Computed Tomography and Its Application to Methanol to Olefin Reactor Beds. *J. Appl. Crystallogr.* **2015**, *48*, 1719–1728.
- (18) Kraft, P.; Bergamaschi, A.; Broennimann, C.; Dinapoli, R.; Eikenberry, E. F.; Henrich, B.; Johnson, I.; Mozzanica, A.; Schlepütz, C. M.; Willmott, P. R.; et al. Performance of Single-Photon-Counting PILATUS Detector Modules. *J. Synchrotron Radiat.* **2009**, *16*, 368–375.
- (19) Vamvakeros, A.; Jacques, S. D. M.; Di Michiel, M.; Senecal, P.; Middelkoop, V.; Cernik, R. J.; Beale, A. M. Interlaced X-Ray Diffraction Computed Tomography. *J. Appl. Crystallogr.* **2016**, *49*, 485–496.
- (20) Ashiotis, G.; Deschildre, A.; Nawaz, Z.; Wright, J. P.; Karkoulis, D.; Picca, F. E.; Kieffer, J. The Fast Azimuthal Integration Python Library: PyFAI. *J. Appl. Crystallogr.* **2015**, *48*, 510–519.
- (21) Kak, A. C. Computerized Tomography with X-Ray, Emission, and Ultrasound Sources. *Proc. IEEE* **1979**, *67*, 1245–1272.
- (22) *MATLAB 2014a*; The MathWorks Inc.: Natick, Massachusetts, United States, **2014**.
- (23) Degen, T.; Sadki, M.; Bron, E.; König, U.; Nénert, G. The HighScore Suite. *Powder Diffr.* **2014**, *29*, S13–S18.
- (24) *Topas*, version 5.0; Bruker AXS: Karlsruhe, Germany, **2012**.
- (25) Yamamoto, O.; Takeda, Y.; Kanno, R.; Fushimi, M. Thermal Decomposition and Electrical Conductivity of $M(\text{OH})_3$ and MOOH ($M=\text{Y}$, Lanthanide). *Solid State Ionics*

- 1985**, *17*, 107–114.
- (26) Fleming, P.; Farrell, R. A.; Holmes, J. D.; Morris, M. A. The Rapid Formation of $\text{La}(\text{OH})_3$ from La_2O_3 Powders on Exposure to Water Vapor. *J. Am. Ceram. Soc.* **2010**, *93*, 1187–1194.
- (27) Wang, F.; Shi, R.; Liu, Z.; Shang, P.; Pang, X.; Shen, S.; Feng, Z.; Li, C.; Shen, W. Highly Efficient Dehydrogenation of Primary Aliphatic Alcohols Catalyzed by Cu Nanoparticles Dispersed on Rod-Shaped $\text{La}_2\text{O}_2\text{CO}_3$. *ACS Catal.* **2013**, *3*, 890–894.
- (28) Chen, G.; Han, B.; Deng, S.; Wang, Y.; Wang, Y. Lanthanum Dioxide Carbonate $\text{La}_2\text{O}_2\text{CO}_3$ Nanorods as a Sensing Material for Chemoresistive CO_2 Gas Sensor. *Electrochim. Acta* **2014**, *127*, 355–361.
- (29) Shafer, M. W.; Roy, R. Rare-Earth Polymorphism and Phase Equilibria in Rare-Earth Oxide-Water Systems. *J. Am. Ceram. Soc.* **1953**, *42*, 563–570.
- (30) Shirsat, A. N.; Ali, M.; Kaimal, K. N. G.; Bharadwaj, S. R.; Das, D. Thermochemistry of $\text{La}_2\text{O}_2\text{CO}_3$ Decomposition. *Thermochim. Acta* **2003**, *399*, 167–170.
- (31) Beruto, D.; Barco, L.; Searcy, A. W.; Spinolo, G. Characterization of the Porous CaO Particles Formed by Decomposition of CaCO_3 and $\text{Ca}(\text{OH})_2$ in Vacuum. *J. Am. Ceram. Soc.* **1980**, *63*, 439–443.
- (32) Mirghiasi, Z.; Bakhtiari, F.; Darezereshki, E. Preparation and Characterization of CaO Nanoparticles from $\text{Ca}(\text{OH})_2$ by Direct Thermal Decomposition Method. *J. Ind. Eng. Chem.* **2014**, *20*, 113–117.
- (33) Jacob, K. T. Solid-State Immiscibility and Thermodynamics of the Calcium Oxide – Strontium Oxide System. **1998**, *81*, 1065–1068.
- (34) Arvanitidis, I.; Du Sichen, D.; Sohn, H. Y.; Seetharaman, S. The Intrinsic Thermal Decomposition Kinetics of SrCO_3 by a Nonisothermal Technique. *Metall. Mater.*

- Trans. B* **1997**, 28, 1063–1068.
- (35) Iwafuchi, K.; Watanabe, C.; Otsuka, R. On the Transition Temperatures of BaCO₃ and SrCO₃ as DTA Temperature Reference Materials. *Thermochim. Acta* **1983**, 64, 381–386.
- (36) Fubini, B.; Torino, U.; Giuria, V. P.; Renzo, F. D. I.; Stone, F. S. Strontianite-Aragonite Solid Solutions Sr_xCa_{1-x}CO₃: Effect of Composition on the Orthorhombic-Rhombohedral Phase Transition and the Conversion to Oxide Solid Solutions Sr_xCa_{1-x}O. *J. Solid State Chem.* **1988**, 77, 281–292.
- (37) Antao, S. M.; Hassan, I. BaCO₃: High-Temperature Crystal Structures and the *Pmcn* → *R3m* Phase Transition at 811°C. *Phys. Chem. Miner.* **2007**, 34, 573–580.
- (38) Zhang, Y.; Yang, G.; Chen, G.; Ran, R.; Zhou, W.; Shao, Z. Evaluation of the CO₂ Poisoning Effect on a Highly Active Cathode SrSc_{0.175}Nb_{0.025}Co_{0.8}O₃ in the Oxygen Reduction Reaction. *ACS Appl. Mater. Interfaces* **2016**, 8, 3003–3011.
- (39) Tiemersma, T. P.; Tuinier, M. J.; Gallucci, F.; Kuipers, J. A. M.; Annaland, M. V. S. A Kinetics Study for the Oxidative Coupling of Methane on a Mn/Na₂WO₄/SiO₂ Catalyst. *Appl. Catal. A Gen.* **2012**, 433–434, 96–108.
- (40) Salehi, M.-S.; Askarishahi, M.; Godini, H. R.; Görke, O.; Wozny, G. Sustainable Process Design for Oxidative Coupling of Methane (OCM): Comprehensive Reactor Engineering via Computational Fluid Dynamics (CFD) Analysis of OCM Packed-Bed Membrane Reactors. *Ind. Eng. Chem. Res.* **2016**, 55, 3287–3299.
- (41) Morgan, K.; Tuitou, J.; Choi, J. S.; Coney, C.; Hardacre, C.; Pihl, J. A.; Stere, C. E.; Kim, M. Y.; Stewart, C.; Goguet, A.; et al. Evolution and Enabling Capabilities of Spatially Resolved Techniques for the Characterization of Heterogeneously Catalyzed Reactions. *ACS Catal.* **2016**, 6, 1356–1381.

- (42) Lomonosov, V. I.; Sinev, M. Y. Oxidative Coupling of Methane: Mechanism and Kinetics. *Kinet. Catal.* **2016**, *57*, 647–676.
- (43) O'Brien, M. G.; Jacques, S. D. M.; Di Michiel, M.; Barnes, P.; Weckhuysen, B. M.; Beale, A. M. Active Phase Evolution in Single Ni/Al₂O₃ Methanation Catalyst Bodies Studied in Real Time Using Combined μ -XRD-CT and μ -Absorption-CT. *Chem. Sci.* **2012**, *3*, 509.

TOC Graphic

